International Conference on Space Optics—ICSO 2004

Toulouse, France

30 March–2 April 2004
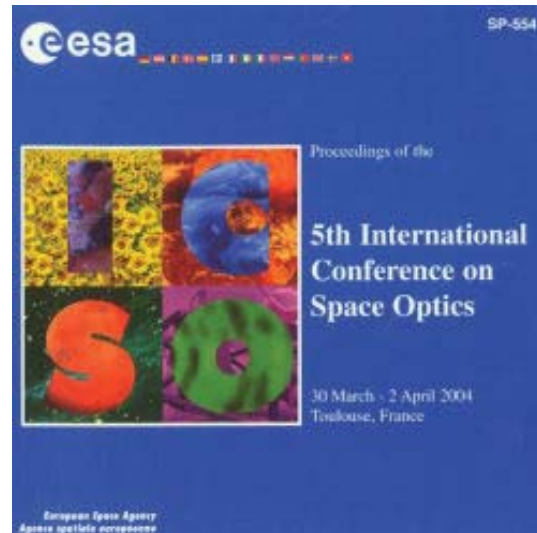
Preliminary calibration results of the wide angle camera of the imaging instrument OSIRIS for the Rosetta mission

V. Da Deppo, G. Naletto, P. Nicolosi, P. Zambolin, et al.

PRELIMINARY CALIBRATION RESULTS OF THE WIDE ANGLE CAMERA OF THE IMAGING INSTRUMENT OSIRIS FOR THE ROSETTA MISSION

V. Da Deppo[(1)], G. Naletto[(1)], P. Nicolosi[(1)], P. Zambolin[(1)], M. De Cecco[(2)], S. Debei[(2)], G. Parzianello[(2)],
P. Ramous[(2)], M. Zaccariotto[(2)], S. Fornasier[(3)], S. Verani[(3)], N. Thomas[(4)], P. Barthol[(5)], S.F. Hviid[(5)],
I. Sebastian[(5)], R. Meller[(5)], H. Sierks[(5)], H.U. Keller[(5)], C. Barbieri[(3)], F. Angrilli[(2)], P. Lamy[(6)], R. Rodrigo[(7)],
H. Rickman[(8)], K.P. Wenzel[(9)]

[(1)] *Department of Information Engineering, University of Padova, CISAS, INFM, Italy, E-mail: dadeppo@dei.unipd.it*
[(2)] *Department of Mechanical Engineering, University of Padova, CISAS, Italy*
[(3)] *Department of Astronomy, University of Padova, CISAS, Italy*
[(4)] *Dept. of Space Research and Planetology, Physikalisches Institut, Bern, Switzerland*
[(5)] *Max-Planck-Institut fuer Aeronomie, Germany*
[(6)] *Laboratoire d'Astronomie Spatiale, France*
[(7)] *Institute for Astrophysics, Granada, Spain*
[(8)] *Astronomical Observatory, Uppsala, Sweden*
[(9)] *ESTEC, ESA, The Netherlands*

ABSTRACT

Rosetta is one of the cornerstone missions of the European Space Agency for having a rendezvous with the comet 67P/Churyumov-Gerasimenko in 2014. The imaging instrument on board the satellite is OSIRIS (Optical, Spectroscopic and Infrared Remote Imaging System), a cooperation among several European institutes, which consists of two cameras: a Narrow (NAC) and a Wide Angle Camera (WAC).

The WAC optical design is an innovative one: it adopts an all reflecting, unvignetted and unobstructed two mirror configuration which allows to cover a $12° \times 12°$ field of view with an F/5.6 aperture and gives a nominal contrast ratio of about 10^{-4}.

The flight model of this camera has been successfully integrated and tested in our laboratories, and finally has been integrated on the satellite which is now waiting to be launched in February 2004.

In this paper we are going to describe the optical characteristics of the camera, and to summarize the results so far obtained with the preliminary calibration data. The analysis of the optical performance of this model shows a good agreement between theoretical performance and experimental results.

1. INTRODUCTION

Rosetta is an ESA mission now dedicated to the exploration of the 67P/Churyumov-Gerasimenko comet. The main mission objective is to study the evolution of the nucleus of the comet and of its environment from 3-4 AU to perihelion. The Rosetta spacecraft will experience a rather long interplanetary journey, about 10 years, with also one Mars and three Earth gravity assists, before reaching the comet in 2014.

The scientific payload of the mission consists of both remote and in situ instruments. Among the remote imaging instruments, OSIRIS is a double camera comprising a narrow angle camera, NAC, and a wide angle camera, WAC. The NAC [1], with is high spatial resolution, is able to study the comet surface in great detail; the WAC, thanks to its large field of view, is able to image the limb and the coma, so to give information mainly on gas and dust outflow directly above the comet nucleus surface [2].

For this purpose, the system has to satisfy a set of scientific requirements [3,4,5], and the most important are: to see the whole comet, a large field of view ($12°$ x $12°$) is needed; to study the dust and continuum properties, the wavelength range has to span from UV through visible (250-750 nm); the achievable optical performance required is that more than 80% of the energy has to be concentrated inside one pixel of the detector; to see properly the coma features together with the bright nucleus surface, the contrast ratio has to be at least 10^{-4}.

To cope with the requirements several optical designs have been considered, but finally it was mandatory to adopt a novel and peculiar off-axis configuration.

2. WAC OPTICAL DESIGN AND PERFORMANCE

The WAC final configuration is a two-mirror off-axis design, unobstructed and unvignetted, having a highly aspheric off-axis primary mirror coupled to an almost spherical secondary one [3]. The corrected field of view is rather wide ($12°$ x $12°$), the focal length is nominally 140 mm and the adopted detector is a CCD by E2V (formerly EEV-Marconi), the CCD42-40, with 2048 x 2048 squared pixel with 13.5 µm side. The optical layout of the system and the complete optical characteristics are visible respectively in Fig. 1 and in Tab. 1.

The choice to have the aperture stop of the system placed on the secondary mirror gives the possibility to

achieve a good optical aberration balancing all over the field of view; however it introduces an in field straylight source to be dealt with the baffling system [6].
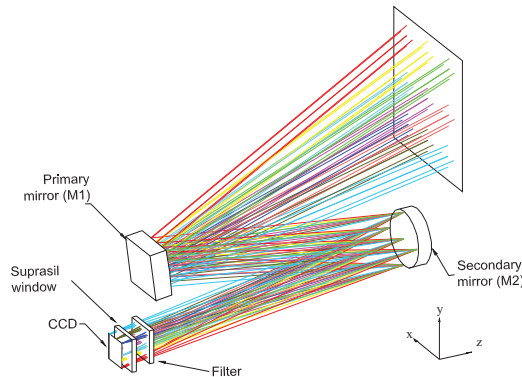
Fig. 1 WAC optical layout.

Tab. 1 WAC optical characteristics.

Optical concept	All-reflective, two-mirror, 20° off-axis, unobstructed, unvignetted
Effective focal length (EFL)	$f_t = 132$ mm , $f_s = 140$ mm
Entrance pupil diameter	25 mm
Focal ratio	F/5.6
Field of view	12° x 12°
Spectral range	230-750 nm
Refocusing	No refocusing necessary from 1 km to ∞
Detector	CCD - 2048 x 2048 pixel
Pixel size	13.5 µm x 13.5 µm
Scale	20" per pixel (average)
Optical quality (EE)	≈80% inside 1 pixel
Filters	Two filter wheel with 7 filters each one
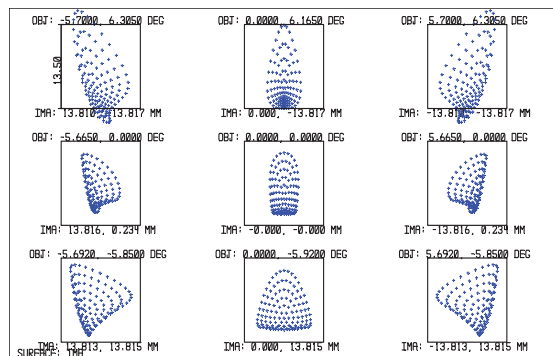
Fig. 2 WAC spot diagrams for the center, the edges and corners of the CCD. The overlapped boxes correspond to the actual pixel size of the detector (13.5 µm).

The optical quality of the design can be evaluated by means of a raytracing code in terms of spot diagrams and of Ensquared Energy (EE) collected by a pixel.

It's clearly visible (Fig. 2) that, for the majority of the field of view (FoV), the spot diagrams are entirely enclosed in a box with dimensions equal to the pixel size. It can also be observed that, even taking into account the diffraction effect, more important at longer wavelengths, the EE inside the pixel is always more than 80 % (Fig. 3).
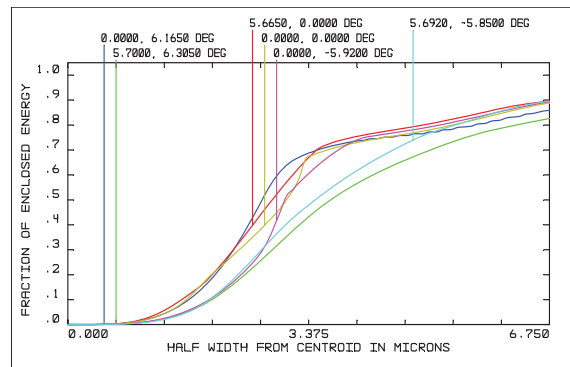
Fig. 3 Ensquared energy scaled by diffraction limit at a wavelength of 640 nm.

To estimate the system performance, it is also very useful to calculate the full width at half maximum (FWHM) of the PSF, using a bi-dimensional Gaussian fit. In fact the ratio of the FWHM, measured along two orthogonal axes, can indicate the presence of residual astigmatism or other asymmetrical aberration. The expected results at a wavelength of 640 nm are shown in Tab. 2. The FWHM are of the order of a third or half of a pixel all over the FoV: comparing the FWHM in x and y direction, a residual astigmatism is noticeable.

Tab. 2 PSF FWHM at 640 nm for different FoVs (X_an,Y_an).

X_an (°)	Y_an (°)	FWHM_x (px)	FWHM_y (px)
0.000	6.165	0.28	0.36
5.700	6.305	0.30	0.55
0.000	0.000	0.27	0.44
5.665	0.000	0.27	0.38
0.000	-5.920	0.34	0.42
5.692	-5.850	0.33	0.48

Being an off-axis design, the system suffers mainly of anamorphic distortion. This means that the system has two different focal lengths in the tangential and sagittal plane (f_t=132 mm, f_s=140 mm), so that a circular object will be imaged as an ellipse with the semiaxis proportional to the focal lengths.

The WAC includes also a set of 14 filters, distributed on two independent wheels, with both narrow and wide bands filters for observation of gas emission lines and of the nearby continuum diffused by the comet dust.

To protect the CCD from the hazardous environmental radiations encountered during the long journey to the comet, a 4 mm thick suprasil window placed right in front of the CCD has been foreseen. Both the filters and the window are in converging light beam (see Fig. 1) so it has been necessary to account for the focal shift they introduce at different wavelengths. To avoid to change detector position, the filter thicknesses have been calculated in order to keep fixed the focus position for each filter; in this calculation, also the dispersion introduced by the suprasil window has been included.

It is worth to mention that the camera has a Front Door Mechanism (FDM), which closes the camera and protects the optics from the dust comet environment, and a high speed shutter (SHM) [7], which allows exposure times as short as 10 msec with very high repeatability and response uniformity. A sketch of the opto-mechanical design of the camera is shown in Fig. 4.
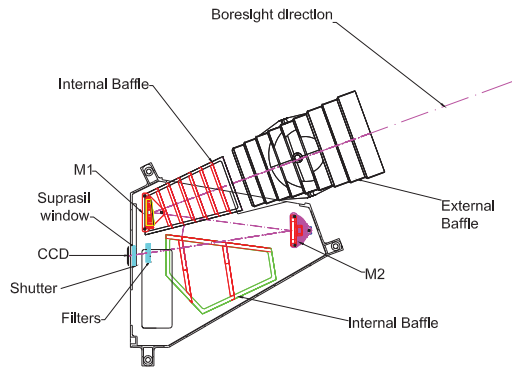
Fig. 4 WAC opto-mechanical design scheme.

3. EXPERIMENTAL SETUP

Both in air and in vacuum tests have been performed to align and calibrate the system. The alignment and preliminary calibration have been done in air at the Padova University (Italy), while the final geometrical and scientific calibrations have been performed in vacuum at the Max-Planck-Institut für Aeronomie in Lindau (Germany). In both institutes, *ad-hoc* facilities have been set in 100-1000 class cleanrooms.

A schematic of the experimental setups used respectively for the calibration in air and in vacuum is shown in Fig. 5 and Fig. 6. In the first, a He-Ne laser at 632.8 nm has been focused on a 10 µm pinhole, acting as a point source placed in the focus of an off-axis parabolic mirror. This optical system was rigidly mounted and worked as a fixed collimator. For scanning the whole field of view of the camera, a dual stage remotely controlled rotating system has been design. This device allows rotations of the camera around two orthogonal axes: one perpendicular to the

tangential plane, defining the azimuth angle (Az); the other in the tangential plane and perpendicular to the boresight direction, defining the elevation angle (El). The absolute precision of the angular position reachable with this rotating stages has been measured to be better than 0.01°.
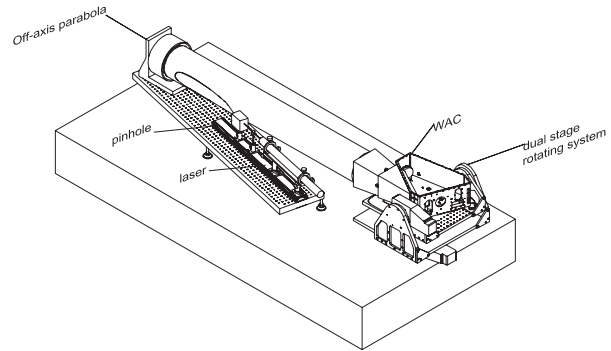
Fig. 5 Schematic of the laboratory facility used for testing the in-air WAC optical performance.
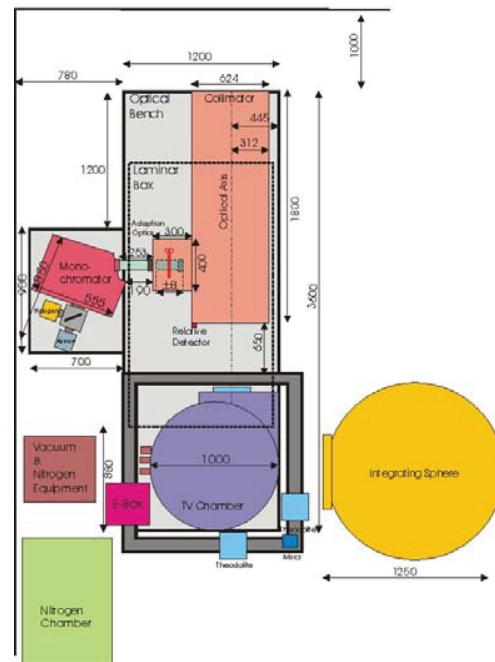
Fig. 6 Schematic of the laboratory facility used for testing the in-vacuum WAC optical performance.

For aligning the camera, a laboratory detecting system has been designed: it consists of a lab CCD camera coupled with a 10X zoom. The lab camera has 1300 x 1030 squared pixel with 6.7 µm side and has been mounted on a XYZ translation stage to scan the whole focal plane. With this setup a flight CCD pixel is sampled 20x20 times, so allowing to have extremely detailed information on the optical quality, in particular

on the aberration being present. With this system we measured the PSF FWHM and the EE with (flight) subpixel resolution.

Before integrating the focal plane assembly, a check of the reached alignment has also been done by means of an interferometer, so to quantify the residual primary aberrations present. The interferometric configuration used is shown in Fig. 7.
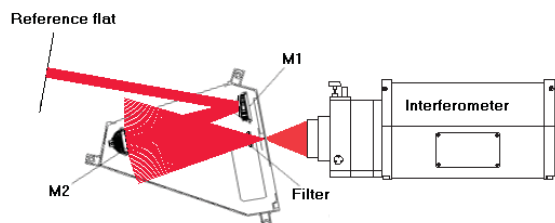
Fig. 7 Interferometric setup for alignment checking.

After integration, with the in-air setup, the measurements of the PSF and of the distortion all over the field of view have been done with the flight CCD at ambient temperature. Taking into account that the operational temperature range of the camera is: 7-17 °C (280-290 K), all the in air measurements have been done in cleanroom at 15 °C.

To test the WAC at its nominal operating temperature, and primarily to have the possibility to operate the CCD at its nominal working temperature (180 K), the in-vacuum (see Fig. 6) optical setup has been used. This setup was conceived to fully calibrate the instrument, which means it was possible to do geometrical, spectral and radiometric calibrations.

The vacuum chamber was equipped with a big optical window, the WAC was mounted on a tip-tilt table for scanning the FoV, and the CCD was cooled down by means of a cold plate facing the CCD radiator.

For the geometrical calibration a motorized XYZ stage could hold, and precisely translate through focus with 0.5 µm steps, a set of pinholes placed in the focus of an off-axis parabolic mirror; a halogen or a xenon lamp was used to illuminate the pinholes. For the spectral calibration the setup was the same except that a monochromator was used to feed the pinholes.

For radiometric measurement, a big 1 m diameter integrating sphere was used to illuminate the camera; to cover all the camera wavelength range both halogen and xenon calibrated lamps could be used.

4. WAC OPTICAL PERFORMANCE

The evaluation of the performance of the camera was done with both the experimental setups described in the previous section; first in air and then in vacuum. The alignment and the preliminary calibration of the system have been performed in air, while the final calibration of the system has been done in vacuum.

In this section we are going to describe the results so far obtained, as not all the data have been analyzed yet. Starting from the discussion of the measured PSF characteristics, we will describe focus and distortion measurement results, and finally we will present an unexpected and unwanted effect seen on flat field images due to a problem on the UV filter coating.

4.1   PSF measurement

At first, after aligning the system, the PSF has been measured all over the FoV using the lab CCD camera; with this experimental setup one pixel of the flight CCD (13.5 µm) corresponds to 20x20 pixels of the lab CCD camera. In this way, the sampling of the PSF features is good giving the capability of discerning very easily the optical quality of the image. Using a bi-dimensional Gaussian fit, the centroid of the image and the PSF FWHM have been measured, and the EE has been estimated.

Tab. 3 PSF FWHM and EE measured all over the FoV.

Az (°)	El (°)	FWHM_x(px)	FWHM_y(px)	EE (%)
-5.0	0.0	0.38	0.37	86.6
-4.0	0.0	0.31	0.45	86.5
-3.0	0.0	0.35	0.43	84.6
-2.0	0.0	0.46	0.41	79.7
-1.0	0.0	0.39	0.46	81.8
0.0	0.0	0.36	0.45	83.2
1.0	0.0	0.41	0.54	81.6
2.0	0.0	0.34	0.56	80.7
3.0	0.0	0.35	0.58	82.8
4.0	0.0	0.37	0.53	84.0
5.0	0.0	0.30	0.31	86.1
6.0	0.0	0.29	0.30	86.9
0.0	-5.8	0.43	0.31	80.9
0.0	-5.0	0.39	0.30	82.9
0.0	-4.0	0.40	0.34	85.1
0.0	-3.0	0.36	0.37	85.6
0.0	-2.0	0.33	0.44	85.2
0.0	-1.0	0.30	0.63	82.4
0.0	1.0	0.45	0.53	83.1
0.0	2.0	0.32	0.55	79.4
0.0	3.0	0.55	0.40	80.0
0.0	4.0	0.49	0.35	80.0
0.0	5.0	0.48	0.36	76.2
0.0	5.8	0.42	0.34	82.4
5.0	-5.0	0.33	0.27	80.1
-5.0	-5.0	0.37	0.39	81.9
-5.0	5.0	0.32	0.29	84.0
5.0	5.0	0.38	0.31	78.7

The values obtained for some point in the FoV are listed in Tab. 3. The FWHM are expressed using the flight CCD pixel size as unit and the EE is obviously calculated inside a flight CCD pixel. The results are in good agreement with theoretical values previously shown, both as for the FWHM and the EE (see Tab. 2 and Fig. 3).

To quantify the residual optical aberration some interferometric measurements have been done using the experimental setup shown in Fig. 7. Through the first nine Zernike coefficients the primary astigmatism, coma and spherical aberration have been calculated. The results are summarised in Tab. 4 together with the estimated FWHM and EE obtained from these interferometric data. As foreseen by the raytracing simulation the main aberration all over the FoV is astigmatism; it can be noticed that also some coma and spherical residual aberrations are present; anyway the calculated FWHM and EE are in accordance with the data foreseen all over the FoV.

Tab. 4 Residual primary aberration, FWHM and EE calculated from interferometric measurements.

Az (°)	El (°)	Ast (λ)	Coma (λ)	Sph (λ)	FWHM _x (px)	FWHM _y (px)	EE (%)
-6	4	0.55	0.21	-0.40	0.31	0.34	81.6
0	4	0.75	0.25	-0.04	0.43	0.39	83.4
6	4	0.29	0.04	-0.19	0.27	0.27	86.8
0	0	0.66	0.19	-0.14	0.29	0.39	79.3
-6	-6	0.29	0.31	0.03	0.29	0.27	87.2
0	-6	0.53	0.25	-0.05	0.33	0.31	86.2
6	-6	0.49	0.12	-0.28	0.30	0.28	83.0
6	-6	0.51	0.11	-0.18	0.32	0.29	83.6
-2	-2	0.48	0.12	-0.39	0.30	0.29	85.3
2	-2	0.61	0.30	-0.36	0.33	0.42	83.3
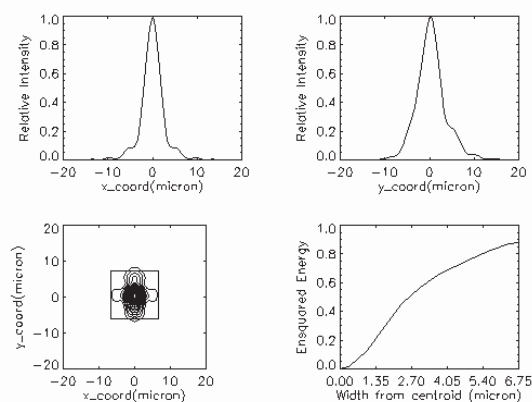
Fig. 8 Theoretical performance at the center of the FoV: PSF cross sections, spot diagram and EE.
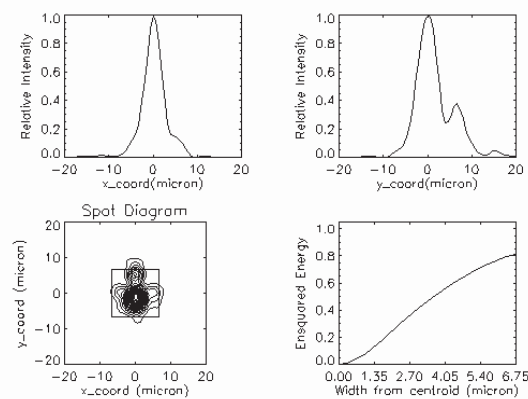
Fig. 9 FM measured optical performance at the center of the FoV: PSF cross sections, spot diagram and EE.

To compare theoretical and actual results at the center of the FoV, the PSF cross section along two orthogonal planes, the spot diagram and the EE calculated from theoretical raytracing data and from measured one are respectively plotted in Fig. 8 and Fig. 9. These plots are very similar, with the measured one presenting slightly more astigmatism and coma then predicted.

After aligning the flight CCD detector a check of the FWHM in all the FoV has been done to verify the performance.

The obtained results are quite surprising, since the FWHM are of the order of 1.4-1.8 px, that is about 4-5 times larger than those measured with the lab CCD camera. Many factors have to be taken into account to explain this results, first of all the undersampling of the image: the features that are going to be measured are smaller than the resolution element, namely the pixel of the detector; therefore the obtained image is the convolution of the actual PSF with the square pixel function. Nevertheless some other factors have to be considered: in fact the expected FWHM after the convolution are of the order of 1.1 px, that is still less than those actually measured. Surely it is difficult to have a reliable Gaussian fit with only 3-5 points and lastly the intra-pixel diffusion/scattering has to be considered.

When using the flight detector, it was possible to reconstruct the actual PSF only by means of the pixel dithering techniques [8]: the pinhole is shifted in the collimator focal plane in steps that move the image on the WAC focal plane less than a pixel. The images obtained are then summed to get a sub-pixel sampled PSF.

4.2 Through focus measurements and focus stability versus temperature

With the vacuum setup a series of through focus measurements has been done at ambient temperature, with the camera and the CCD at ambient temperature, but also with the CCD cold, and during the cooling

down and warming up of the CCD itself. All these measurements are really interesting.

In fact, there was a problem with the camera software (GSE) commanding the heaters so that it was impossible to keep the camera at its right operational temperature. Actually when the CCD was cooling down also the camera was cooling down below its operational temperature; so that much of the measurements taken with cold CCD have also a cold camera structure. This not wanted event has been useful giving the possibility to observe the behaviour of the focus position as a function of the camera structure temperature.

The through focus measurements have been done by means of the motorized stage supporting the pinhole. To simulate a source placed at different distance from the camera, the pinhole has been moved back and forth along the optical axis of the collimator starting at the off axis parabola focus position. Being known the collimator focal length and the focal length of the camera, it was possible to calculate the object distance at which the camera was focused and than estimate the position of the WAC focus for a source placed at infinity.

In the through focus measurements plot the value of the FWHM of the PSF, measured for different pinhole positions, is plotted as a function of defocus, so to estimate the position of the focus with respect to the actual detector position.

The through focus measurements have been done at the center of the FoV where, as already explained, the system is astigmatic; this astigmatism is clearly visible in the through focus measurements plots (figs. 11-13) where both FWHM in x, y and the mean are shown.

A lot of through focus measurements have been done, giving the proof that the position of the focus is dependent on the camera structure temperature and that also some minor dependence on CCD temperature is present, especially at lower ones (see Fig. 10).

In Fig. 11 a through focus measurement at ambient temperature is shown. The CCD was at 293 K while the structure was at 290 K. In addition to the evident astigmatism, it's also noticeable that the focus is shifted of about 100 μm from the nominal position (which corresponds to have a system focused for a source placed at 200 m from the camera).
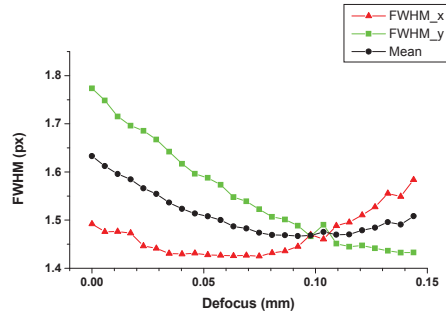
Fig. 11 Through focus measurements at ambient temperature. FWHM in x and y direction and mean values are plotted.
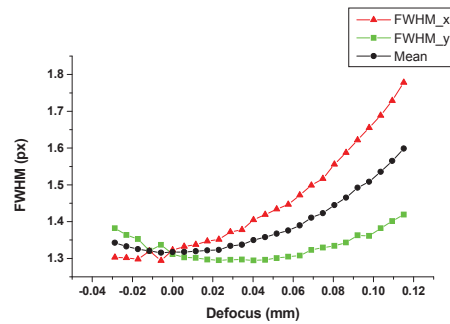
Fig. 12 Through focus measurements for CCD and structure at nominal operating temperature.
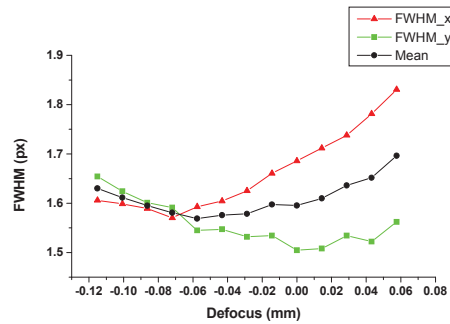
Fig. 13 Through focus measurements keeping cold both CCD and structure.

In Fig. 12 another situation is presented, with the structure at 280 K and the CCD at 190 K corresponding to the nominal working condition. In

Fig. 10 WAC defocus versus CCD and structure temperature. The temperature of the structure is shown as label to the measurement points.

this case the camera is in its nominal focus position or, saying it in other words, it is rightly focused at infinity. With the temperature of the structure going down outside the operational range, the focus position is gradually moving, till the system is in focus for a virtual object (see Fig. 13).

An estimate of the expected focus shift has been calculated for an isothermal structure taking into account the coefficient of thermal expansion both of aluminium, the material in which the structure has been made, and of the BK7, the material used for the mirror. The values of the defocus obtained are of the order of 90 µm for a 10 K variation of the temperature: this is in good agreement with the measurements, taking also into account the temperature gradients definitely present in the system.

To ascertain the main responsible of the focus shift are variations of the temperature of the structure, some measurements have been done heating the camera structure to 280-285 K that is the nominal working temperature. It has been seen that for a 10 K variation of the structure temperature, there is about 100 µm defocus variation, as expected.

Also a check of the focus position for all the filter has been done: it has been verify that the focus is stable within 20 µm when the camera structure is kept at constant temperature.

4.3   Distortion

The distortion measurements have been done with the WAC in the vacuum chamber mounted on the tip-tilt table. On this table there was also a big reference cube that allowed to measure the camera orientation, in terms of azimuth and elevation, by means of two theodolites.
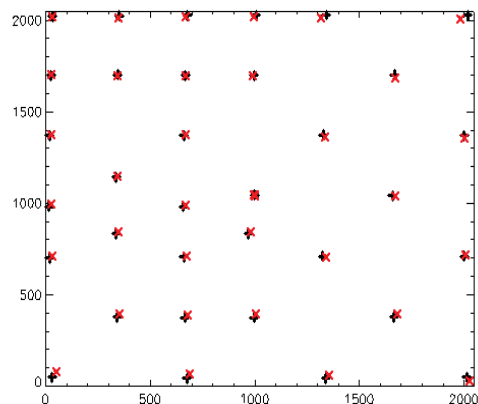
Fig. 14 Theoretical distortion (+) versus measured one (x). The difference between the two has been multiplied by a factor 20 to be visible.

The position of the spot on the CCD has been calculated, as done for the PSF measurements, fitting

the PSF with a bi-dimensional Gaussian and taking the centroid as reference. The Az and El values are referred to the center of the FoV and the theoretical positions have been determined by a raytracing simulation.

Plotting the differences between actual positions and foreseen ones, it was possible to see a residual rotation between the two maps due to the misalignment of the cube reference axes to the camera ones. Removing this effect the differences between the expected and measured distortion are always less than 1.5-1.6 px all over the field of FoV.

The accordance between predicted distortion and actual one can be seen in Fig. 14, where the differences are plotted in function of the FoV and have been multiplied by a factor twenty to be visible.

4.4   Filter defects

The filters are located on two wheels close to the detector and there are 7 filters per each wheel. The filters have spectral bands ranging from UV to visible and some of them have narrow bandwidth (4 nm). Different substrates have been used for the filters: those in the visible range are coloured glasses, while those in the UV range are made of suprasil. The UV filters are difficult to be manufactured because, having the substrate no blocking effects, the selection of the wavelengths has to be done only by the interferential coating; this means that the multilayer has to be realized by more than one hundred layers.

Fig. 15 Flat field image acquired illuminating the camera with the integrating sphere using the halogen lamps. The used filter is one with UV bandpass.

Unfortunately, some of the UV filters present some defects on the coatings that have been visible during the acquisitions of the flat fields. Using the integrating sphere with the halogen lamps to illuminate the WAC, images like that in Fig. 15 can be seen. The filter used for this image is the OH, which has the transmission

peak at 308.5 nm and a bandwidth of 4 nm: in principle no visible light should have been seen by the detector. From the analysis of this and other similar images, it has been understood that the bright circles are images of the secondary mirror (M2) of the camera imaged through some pinholes on the coating of the filters (the holes on the filters act as a pinhole camera). Giving the distance of the detector and the size and distance of M2, the diameter of the circles has been estimated to be of the order of 670 px (9 mm) exactly like the size of the circles actually seen.

5. CONCLUSIONS

In this paper we have at first briefly described the optical design and the theoretical performance of the WAC for the Rosetta mission. Then, the preliminary results of the calibration of the flight model of the camera have been reported. The results show a good agreement between predicted and measured performance.

The calibration measurements have been done in two steps: alignment and preliminary calibration have been performed with a setup designed to work with the WAC in air; final calibration has been performed with a setup having the camera placed in a vacuum chamber. Since the camera is pixel limited, the spot size is less than the pixel size. The PSF has to be measured with an *ad-hoc* laboratory setup capable of magnifying the PSF. With this system we have seen that the PSF is very similar to the nominal one and that the EE is about 80 % all over the FoV.

With the vacuum setup we have verified that the system works nominally inside its working temperature range. Also the distortion has been measured proving that it is really very similar to the prediction, being the differences between theoretical and measured position less than a 1.5 px even at the edges of the FoV.

Finally, during flat fielding acquisition, a problem related to the UV filter coating has been discovered. Some pinholes on the coating let some visible light to pass through, giving rise to some circles on the images. At present we are working on this problem trying to find a way to recover the flat field images.

Even if not all the data have been analysed yet, we can conclude that the performance of the flight model of the WAC is optimal and that it is essentially compliant with expectations.

6. REFERENCES

1. Castel D., Calvel B., Lamy P. L., Dohlen K., Bougoin M., Monolithic SiC telescope of the OSIRIS Narrow-Angle Camera for the cometary mission ROSETTA, in Advanced Telescope Design, Fabrication, and Control, *Proc. SPIE*, Vol. 3785, 56-65, 1999.

2. Thomas N., Keller H. U., Arijs E., Barbieri C., Grande M., Lamy P., Rickman H., Rodrigo R., Wenzel K.-P., A'Hearn M. F., Angrilli F., Bailey M., Barucci M. A., Bertaux J.-L., Brieß K., Burns J. A., Cremonese G., Curdt W., Deceuninck H., Emery R., Festou M., Fulle M., Ip W.-H., Jorda L., Korth A., Koschny D., Kramm J.-R., Kührt E., Lara M.L., Llebaria A., Lopez-Moreno J. J., Marzari F., Moreau D., Muller C., Murray C., Naletto G., Nevejans D., Ragazzoni R., Sabau L., Sanz A., Sivan J.-P., Tondello G., OSIRIS-The optical, Spectroscopic and Infrared Remote Imaging System for the Rosetta orbiter, *Adv. Space Res.*, Vol. 21(11), 1505-1515, 1998.

3. Naletto G., Da Deppo V., Pelizzo M. G., Ragazzoni R., Marchetti E., Optical design of the Wide Angle Camera for the Rosetta mission, *Appl. Opt.*, Vol. 41(7), 1446-1453, 2002.

4. Da Deppo V., Naletto G., Nicolosi P., Zambolin P., Pelizzo M. G., Barbieri C., Optical performance of the wide-angle camera for the Rosetta mission: preliminary results, in "UV/EUV and Visible Space Instrumentation for Astronomy and Solar Physics", *Proc. SPIE*, Vol. 4498, 248-257,2001.

5. Naletto G., Da Deppo V., Nicolosi P., Zambolin P., Barbieri C., Fornasier S., Calibration of the wide-angle camera for the Rosetta mission: preliminary results on the flight model, in "Future EUV-UV and Visible Space Astrophysics Missions and Instrumentation", *Proc. SPIE*, Vol. 4854, 375-384, 2003.

6. Debei S., Fornasier S., Ramous P., Barbieri C., Da Deppo V., Brunello P., Peron F., The Wide Angle Camera of the Rosetta mission: design and manufacturing of a innovative baffling system for an aspherical optics telescope, in "UV/EUV and Visible Space Instrumentation for Astronomy and Solar Physics", *Proc. SPIE*, Vol. 4498, 324-334, 2001.

7. De Cecco M., Debei S., Guizzo G. P., Pertile M., Zaccariotto M., Angrilli F., Barbieri C., High-performance shutter for space applications, in "Optomechanical Design and Engineering 2002", *Proc. SPIE*, Vol. 4771, 186-197, 2002.

8. Poletto L., Nicolosi P., Enhancing of the spatial resolution of a two-dimensional discrete array detector, *Opt. Eng.*, Vol. 38(10), 1748-1757, 1999.